Corrosion of Magnesium Alloy AZ31 Coated by Plasma Electrolytic Oxidation

O. O. Kalinichenko[a], V. O. Holovenko[a], K. V. Roienko[a], D. O. Misnyankin[a],
O. B. Girin[a], and L. O. Snizhko[a], *

[a]*Ukrainian State University of Chemical Technology, Dnipro, 49005 Ukraine*
*e-mail: lsnizhko@gmail.com

Abstract—In this work, plasma electrolytic oxidation was performed on AZ31 magnesium alloy. The electrolytes contained mixtures of sodium silicate, sodium hexamethaphosphate, potassium hydroxide, and potassium fluoride. Scanning electron microscopy, X-ray diffraction, porosity measurements, atomic analysis, and exposition in 3% NaCl were carried out to investigate the microstructure, elemental/phase composition, and corrosion resistance of the coatings. The results showed that the coating formed in both silicate- and phosphate-containing electrolyte were mainly composed of MgO, $Mg(OH)_2$, Mg_2SiO_4, and $Mg_3(PO_4)_2$ showing the most dense structure and the best corrosion resistance.

INTRODUCTION

Magnesium and its alloys have a number of unique properties—high specific strength, the ability to absorb impact and vibration, good machinability, and low density. Magnesium is widely distributed in nature and is non-toxic, which makes it a valuable structural material in various applications. The proven biocompatibility of magnesium alloys [1] reveals the prospects for their use as implants in orthopaedics and traumatology. Mg alloys have a modulus of elasticity (40–45 GPa)—the closest to the bone (10–40 GPa), which makes them more desirable material than stainless steel and titanium. Another advantage of magnesium alloys is their tendency to biodegradation (gradual dissolution and absorption by a living organism), which contributes to the physiological fusion and tissue reconstruction with a minimal risk of inflammation [2]. This property of magnesium eliminates the need for a second surgical operation to remove implants after tissue repair. Magnesium alloys also exhibit osteoconductive and osteoinductive properties, providing a temporary support during tissue repair. In this sense, they are superior to permanent implants, which can eventually cause physical irritation and chronic inflammatory reactions. It is expected that orthopaedic implants made of magnesium should maintain mechanical integrity for 12–18 weeks (bone healing time) [3]. Meanwhile, pure magnesium quickly dissolves in saline (3% NaCl, pH 7.4–7.6), losing mechanical integrity before the tissue has healed enough. In addition, the dissolution of magnesium is accompanied by the release of hydrogen, the bubbles of which can also cause complications.

Thus, a promising future of magnesium and its alloys depends on the ability to control the rate of corrosion in body fluids.

Several publications [3–5] have indicated that the poor corrosion resistance of Mg alloys results from a high intrinsic dissolution tendency of magnesium, which is only weakly inhibited by corrosion product films, and the presence of second phases acting as local cathodes and thus causing local micro-galvanic acceleration of corrosion. At the same time, corrosion is a positive attribute for Mg alloys to be used as biodegradable implants [6].

Surface modification is one of the most effective ways not only to reduce and control the degradation behaviour but also to improve the surface biocompatibility of Mg-based alloys [7]. Anodic spark deposition (ASD) or plasma electrolytic oxidation (PEO) is a surface treatment process employed to produce relatively thick, ceramic-like coatings on magnesium, aluminium, titanium, and other valve metals, with incorporation of species originating from the substrate and the electrolyte [8]. Coatings are formed at high voltages in sparking mode on the metal surface.

The local high temperature in the discharges facilitates the formation of high-melted phases. The formation of coatings involves chemical, thermal, and anodic oxidation processes. ASD processing exhibits advantages of high throwing power, simple non-toxic electrolytes, minimum requirements for pre-treat-

Table 1. Composition of the alloy AZ31

Elements	Al	Zn	Mn	Si	Fe	Cu	Ni	Ca	Others	Mg
Min %	2.50	0.60	0.20							Balance
Max %	3.50	1.40	1.00	0.10	0.005	0.05	0.005	0.04	0.3	

Table 2. Composition of electrolytes

Components	Electrolytes, g L^{-1}		
	1	2	3
Sodium trisilicate (Na$_2$O · 3SiO$_2$, density 1.49 g cm^{-3})	10	10	–
Potassium hydroxide (KOH)	4	4	4
Sodium hexametaphosphate (NaPO$_3$)$_6$	2	2	5
Sodium fluoride (NaF)	–	2	4

ment, and formation of coatings with a relatively hard surface, corrosion and wear resistant. ASD of magnesium alloys is normally performed in alkaline electrolytes with inorganic polymers. As usual, coating contains amorphous and/or crystalline phases such as MgO, Mg$_2$SiO$_4$, Mg$_3$(PO$_4$)$_2$ [8]. The respective literature also contains information on the suitability of sodium aluminate solutions for the formation on magnesium MgAl$_2$O$_4$ type spinel with a melting point of 2135°C [9]. Silicate- [10] and and phosphate- [11] containing electrolytes are widely used [12], allowing to obtain the smoothest and most uniform coatings. The type of anions affects the rate of their migration in the electrolyte, as well as the diameter and depth of the pores formed. Alkalis (KOH or NaOH) are used to increase the conductivity and to regulate the pH of solutions. The thickness of the coatings, as usual, is in a range of 50−100 μm, with an average growth rate of 1−5 μm min^{-1}.

The structure of the coatings is determined by five main factors: chemical compositions of the electrolyte and of the alloy, current density, electrical processing regime, and duration of the process. As a rule, the surface of PEO coatings has a fairly coarse porous structure and needs subsequent removal of the top layer, or to be sealed. It was considered [12] that spherical pores of PEO coatings surrounded by a halo of fused material are formed by outgoing gases. So, any measures limiting gas generation at the electrode and contributing to a decrease in temperature on the surface of the coating will positively affect the morphology of the surface.

It was found elsewhere that the coatings obtained from alkaline silicate (10 g L^{-1} Na$_2$SiO$_3$ + 1 g L^{-1} KOH) and phosphate (10 g L^{-1} Na$_3$PO$_4$ + 1 g L^{-1} KOH) electrolytes by the pulses with equal anodic and cathodic current densities 600 A m^{-2} were different [13]. A "phosphate" coating had a more compact and continuous structure than the "silicate" one. The influence of the solution composition, current density, and time

during the PEO process on the coating morphology and thickness were discussed in [14]. The coatings obtained in electrolytes, consisting of Na$_2$SiO$_4$, Na$_4$P$_2$O$_7$ · 10H$_2$O, KOH, and KF were investigated. An X-ray diffraction (XRD) analysis revealed the presence of amorphous and crystalline phases including MgO, Mg$_3$(PO$_4$)$_2$, and MgSiO$_4$ for treatment in the solution without KF, and MgO and MgSiO$_4$ for the coatings obtained in the electrolyte with the addition of KF. It was found that the coatings have protective properties and reduce the corrosion current density by two orders of magnitude. Besides, the KF containing electrolyte led to formation of thicker coatings [15].

In the present work, a comparative study of the microstructure, phase constituent, corrosion resistance of coatings formed by PEO in silicate-, aluminate-, and phosphate-containing electrolytes was undertaken.

EXPERIMENTAL

Materials

The composition of AZ31 alloy used in this study is presented in the Table 1.

The samples were machined to the dimensions 24 × 24 × 1 mm. Preliminary preparation included degreasing in a warm (40−60°C) solution consisting of 40 g L^{-1} Na$_3$PO$_4$ and 40 g L^{-1} Na$_2$CO$_3$. Then the samples were washed with cold running water.

This study employed three types of the electrolytes presented in Table 2.

The temperature of the electrolyte was maintained in a range of 17−20°C by agitation with a compressed air and circulation of ice water in the water jacket around the bath. Plasma anodizing was performed using a bipolar adjustable pulsed current power supply operated in the galvanostatic mode. The process parameters were fixed as follows: the negative-to-positive
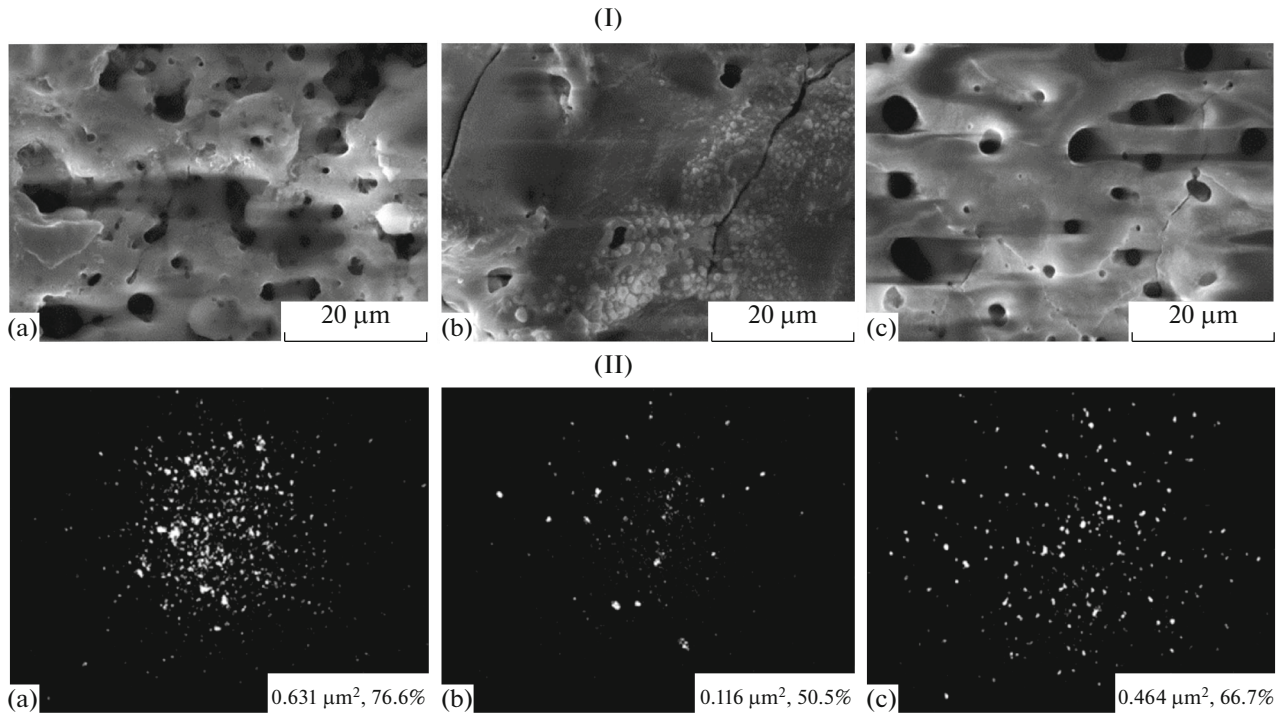
(I)

(II)

Fig. 1. Morphology (I) and porosity (II) of PEO coatings obtained on AZ31 in electrolytes 1 (a), 2 (b), and 3 (c). The average size of the pores (μm^2) and total porosity (%) are placed on the images.

current ratio ($R = I_n/I_p$) was set at 50%, the time of electrolysis was 10 min and the frequency was 100 Hz.

Coating Analysis

Elemental (Mg, Si, P) composition of the coated layer was determined by X-ray fluorescence (XRF) analysis using EXPERT-4L W184U according to the standards DIN EN ISO 3497, and ASTM B 568. The oxygen content was not detected with XRF.

The phase analysis was performed by XRD using a DRON-3 diffractometer (CuK_α radiation). The measurements were done using Bragg—Brentano theta-2theta geometry. The diffraction patterns were recorded within a range from 5° to 100° in 2theta.

The obtained XRD patterns were compared with the JCPDS standards to identify the phase composition. The surface porosity size and porosity distribution were calculated from numerical image analysis using an ImageJ/Fiji 1.46 program.

Corrosion Rate Measurements

Total corrosion tests were performed in a 3% NaCl solution by the hydrogen evolution measurement that was considered to be a real-time measurement of corrosion [16, 17]. The tests were performed during 150 h under the temperature and pressure control. The gas volume V (mL) was reduced to normal conditions by the formula:

$$V_0 = \frac{VT_0\left(P - P_{H_2O}\right)}{TP_0},\qquad(1)$$

where T and P are temperature and pressure under experimental conditions, respectively, P_{H_2O} is the pressure of the saturated water vapour at temperature T.

The volumetric corrosion rate $K_V^{H_2}$ (mL cm^{-2} h^{-1}) was calculated from the slope of the dependencies plotted in the coordinates V_0–t.

RESULTS AND DISCUSSION

Microstructural Characterization

The morphology and porosity images of the coatings obtained on AZ31 in electrolytes 1, 2, and 3 are shown in Fig. 1.

It can be seen that the most continuous, low porous, and entire coating is formed in electrolyte 2. The pores observed are the traces left by the sparks and released gases.

Elemental and Phase Analysis

Elemental composition of the coatings is presented in Table 3.

Table 3. Elemental composition of coatings obtained in electrolytes 1−3

Elements	Composition (at %) of the coatings obtained from electrolytes		
	1	2	3
Mg	48.18	40.18	44.97
Al	5.34	4.50	5.28
Si	21.20	38.84	0.22
P	21.30	11.49	44.14
K	1.16	2.73	3.59
Ca	0.33	0.28	0.19
Mn	0.52	0.37	0.44
Zn	2.01	1.61	2.16

Table 4. R rate of hydrogen release during exposition of AZ31 with coatings in 3% NaCl

Sample	Bare AZ31	Electrolyte 1	Electrolyte 2	Electrolyte 3
$K_V^{H_2}$ (mL cm^{-2} h^{-1})	0.2497	0.0056	0.0053	0.0181

The coatings composition demonstrates competitive adsorption of phosphate and silicate anions (electrolytes 1 and 2). In the absence of silicate anions (electrolyte 3), the adsorption of phosphates significantly increases.

XRD spectra of the coatings obtained from electrolytes 1−3 are presented in Fig. 2.

All coatings show the presence of MgO, Mg(OH)$_2$ and compounds formed from the underlying metal and ions derived from the electrolytes, such as Mg$_2$SiO$_4$, Mg$_3$(PO$_4$)$_2$, and MgF$_2$. This fact suggests a more dense and continuous structure of the coating obtained, for example, in electrolyte 2. In principle, the data obtained here coincide with the results published in [11] and [18], which showed participation of elements Si and P in thermochemical reactions with the underlying metal. The traces of Al$_2$O$_3$ (not shown here) has been find in all coatings. The presence of aluminium oxide can be explained by the role of Al as an alloying element commonly used for modifying the mechanical and corrosion properties of Mg alloys. Addition of Al (1−5%) leads to the reduction of the grain size, dissolving partly in Mg solid solutions. Secondary phase Mg$_{17}$Al$_{12}$ precipitates along the grain boundaries [20].

During plasma stages of electrolysis, direct injection of magnesium metal or cations Mg/Mg^{2+} into the electrolyte can occur through plasma discharge channels. The ejected particles react with OH$^-$ ions, forming the magnesium hydroxide, which is then partially transformed into magnesia. Besides, Mg/Mg^{2+} can directly react with oxygen forming magnesium oxide [15]. For Mg^{2+} to move through the barrier layer, its energy needs to be higher than the sum of the free energy difference between the ion in the metal and in the oxide film.

Fluoride anions chemisorb on the metal surface forming an adsorbed layer MgF$_{ads}^-$ which transforms to magnesium fluoride MgF$_2$. It was supposed elsewhere, that the latter reacts with oxygen by the reaction $MgF_2 + \left[O^{2-}\right] = MgO + 2F^-$ and serves as a catalyst for magnesium oxydation [19].

Formation of Mg$_3$(PO$_4$)$_2$ can be explained by a thermochemical reaction between two oxides (P$_2$O$_5$ and MgO) or ejected magnesium and phosphate anions (Mg^{2+} and PO$_4^{3-}$). The mechanism of this reaction is not entirely clear, but, in any case, the ratio Mg/P has to be 3 : 2.

Corrosion Measurements

The results of a comparative study of the specific volume of hydrogen evolution in 3% NaCl in due course are shown in Fig. 3.

The rate of hydrogen evolution on clear magnesium and on coated samples is linear in time. Minimal corrosion (~50 times less than clear AZ31) was observed on the samples coated in silicate-containing electrolytes. The rate of hydrogen release is presented in Table 4.

The data in Table 3 show that the corrosion rate of coated samples is significantly lower than that of the uncoated one. Coatings obtained from silicate-containing electrolytes have better protective properties.

It was demonstrated elsewhere that in electrolytes, Mg$_{17}$Al$_{12}$ phase, which is presented in Al-containing Mg alloys, exhibits a passive behaviour, acting as a cathode with respect to the α-phase in Mg matrix and acts as a corrosion barrier surrounding the α-Mg
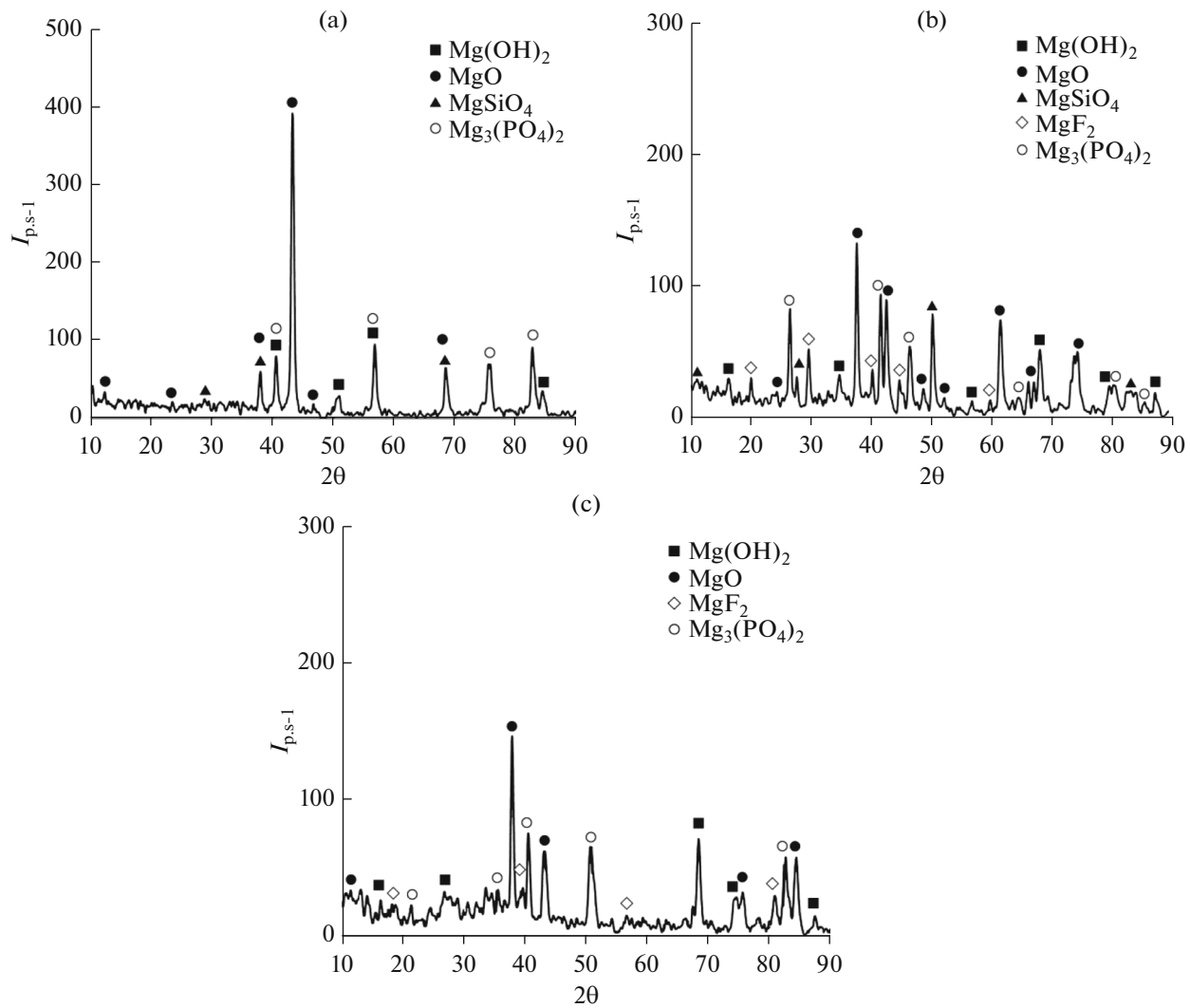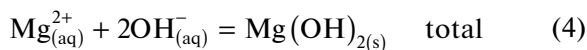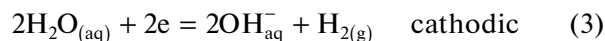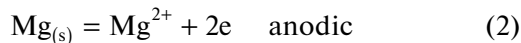
Fig. 2. XRF spectra of coatings obtained in electrolytes 1 (a), 2 (b), and 3 (c).

matrix thereby reducing the corrosion rates [18]. In the corrosive media, the electrochemical dissolution of Mg produces OH^--ions as a result of hydrogen gas formation from the cathodic reaction. It is widely known that corrosion of magnesium in aqueous media proceeds with hydrogen depolarization, while anodic and cathodic reactions occur predominantly on the surface of the metal, partially penetrating into the protective film:

$$Mg_{(s)} = Mg^{2+} + 2e \quad \text{anodic} \quad (2)$$

$$2H_2O_{(aq)} + 2e = 2OH^-_{aq} + H_{2(g)} \quad \text{cathodic} \quad (3)$$

$$Mg^{2+}_{(aq)} + 2OH^-_{(aq)} = Mg(OH)_{2(s)} \quad \text{total} \quad (4)$$

The presence of OH^--ions causes an increase of the local pH at the interface and facilitates the formation and precipitation of MgO and/or $Mg(OH)_2$ as corrosion products [2]. The evolution of 1 mol of hydrogen gas (22.4 L) directly corresponds to the dissolution of 1 mol of Mg (24.31 g). In theory, measuring the volume of H_2 gas produced is equivalent to the result obtained when measuring the mass loss of Mg. It is also possible to determine the degree of alkalization based on the volume of hydrogen evolved if it is assumed that 2 mol of $(OH)^-$ corresponds to 1 mol of oxidized Mg. According to various estimates mentioned elsewhere, this theoretical ratio rather strongly deviates from the practical one (within the range of 0.6 ± 0.08) [16]. In the present study, a comparative study of the corrosion rate of a pure and coated alloy AZ31 was made.

It is known [20] that corrosion of Mg alloys in the 3.5% NaCl solution is typically greater than ~3 mm per year and causes the solution pH to rise to a pH of 10.3 (typically within 2–3 h) because of the precipitation of the sparingly soluble $Mg(OH)_2$. Pitting corrosion was a typical corrosion mode to the dual phase
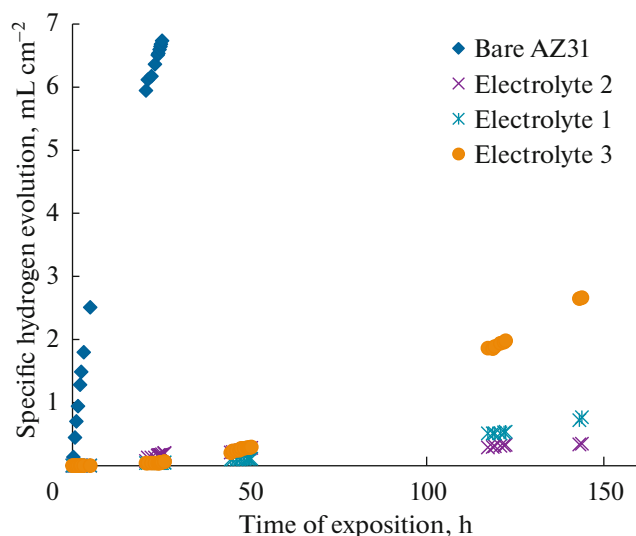
Fig. 3. Kinetic dependences of hydrogen evolution during corrosion of AZ31 alloy with PEO coatings in 3% NaCl: bare alloy (0), alloy with coatings obtained from electrolytes 1−3, respectively.

magnesium alloy because the corrosion potential difference could accelerate the corrosion rate of the low corrosion potential phase. Corrosion pits initiated on the bare α-phase of the samples immersed in NaCl aqueous solution in the initial corrosion stage.

Figure 4 demonstrates the surface of AZ31 alloy after a corrosion test.

It can be seen that the coating obtained in electrolyte 2 remained the most saved with only few pits on the surface. Cl⁻-ions are very harmful to magnesium alloys and accelerate their corrosion. Pitting corrosion was a typical corrosion mode to the dual-phase magnesium alloy because the corrosion potential difference could accelerate the corrosion rate of the low corrosion potential phase [20]. In the presence of chloride ions, poorly soluble magnesium hydroxide is converted to a soluble salt $MgCl_2$ as a result of adsorption displacement of oxygen from the metal surface:

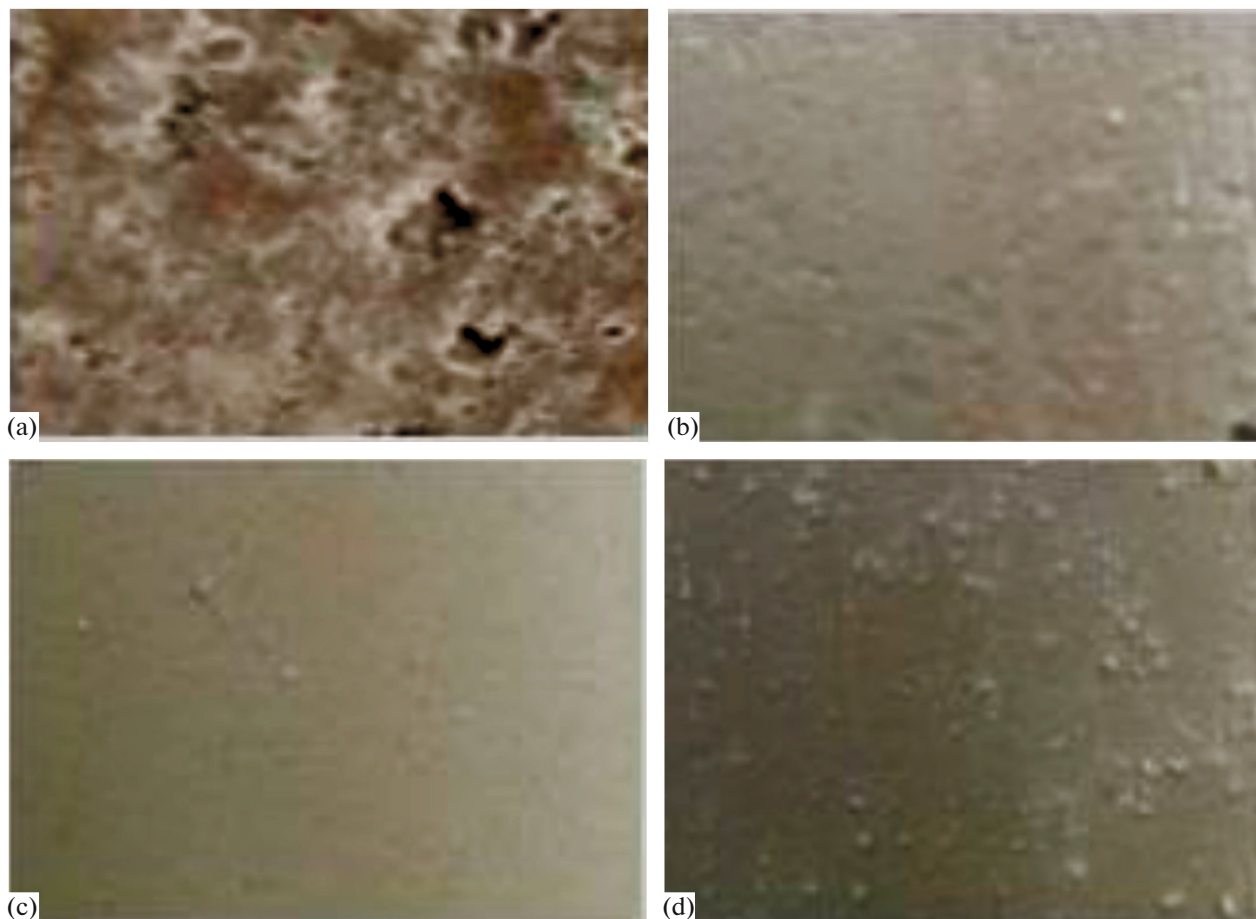$$Mg(OH)_2 + 2Cl^- = MgCl_2 + 2OH^-. \qquad (5)$$

Fig. 4. Surface of AZ31 alloy after corrosion test on: (a) bare AZ31; (b) coated in electrolyte 1; (c) coated in electrolyte 2; (d) coated in electrolyte 3.

After nucleation, corrosion pits continuously extend along the alloy surface while they develop in the direction perpendicular to the alloy surface [21].

It is supposed here that PEO coating prevents the diffusion of both Cl^--ions to the surface of bare alloy and back diffusion of H_2 from the alloy to electrolyte slowing down reactions (2) and (5).

CONCLUSIONS

Protective coatings were deposited on AZ31 magnesium alloy by the PEO process in electrolytes containing sodium silicate, sodium hexamethaphosphate, potassium hydroxide, and sodium fluoride. The coatings were mainly composed of magnesium oxide/hydroxide, Mg_2SiO_4, $Mg_3(PO_4)_2$, and traces of MgF_2. All films exhibited a good protection effect in 3% NaCl. The films obtained in the electrolyte contained a mixture of silicate-, hexamethaphosphate, and fluoride anions, exhibiting the best corrosion resistance (corrosion rate is reduced by 50 times according to measurements of H_2 evolution during 150 h of exposition) due to a relatively small porosity, compact microstructure, and existence of chemical compounds formed by Mg and species derived from the electrolyte.

REFERENCES

1. Witte, F., *Acta Biomater.*, 2015, vol. 23, pp. 28−40.
   https://doi.org/10.1016/j.actbio.2015.07.017

2. Alvarez-Lopez, M., Pereda, M.D., Del Valle, J.A., Fernandez-Lorenzo, M., et al., *Acta Biomater.*, 2010, vol. 6, pp. 1763−1771.
   https://doi.org/10.1016/j.actbio.2009.04.041

3. Staiger, M.P., Pietak, A.M., Huadmai, J., and Dias, G., *Biomaterials*, 2006, vol. 27, pp. 1728−1734.
   https://doi.org/10.1016/j.biomaterials.2005.10.003

4. Stojadinović, S., Vasilić, R., Radić-Perić, J., and Perić, M., *Surf. Coat. Technol.*, 2015, vol. 273, pp. 1−11.
   https://doi.org/10.1016/j.surfcoat.2015.03.032

5. Song, G., *Corros. Sci.*, 2007, vol. 49, pp. 1696−1701.
   https://doi.org/10.1016/j.corsci.2007.01.001

6. Atrens, A., Liu, M., and Zainal Abidin, N.I., *Mater. Sci. Eng., B*, 2011, vol. 176, pp. 1609−1636.
   https://doi.org/10.1016/j.mseb.2010.12.017

7. Witte, F. and Eliezer, A., in *Degradation of Implant Materials*, New York: Springer-Verlag, 2012, pp. 93−109.
   https://doi.org/10.1007/978-1-4614-3942-4_5

8. Arrabal, R., Matykina, E., Hashimoto, T., Skeldon, P., et al., *Surf. Coat. Technol.*, 2009, vol. 203, pp. 2207−2220.
   https://doi.org/10.1016/j.surfcoat.2009.02.011

9. Curran, J.A. and Clyne, T.W., *Surf. Coat. Technol.*, 2005, vol. 199, pp. 177−183.
   https://doi.org/10.1016/j.surfcoat.2004.11.045

10. Cai, Q., Wang, L., Wei, B., and Liu, Q., *Surf. Coat. Technol.*, 2006, vol. 200, pp. 3727−3733.
    https://doi.org/10.1016/j.surfcoat.2005.05.039

11. Ng, W.F., Chiu, K.Y., and Cheng, F.T., *Mater. Sci. Eng., C*, 2010, vol. 30, pp. 898−903.
    https://doi.org/10.1016/j.msec.2010.04.003

12. Khaselev, O., Weiss, D., and Yahalom, J., *Corros. Sci.*, 2001, vol. 43, pp. 1295−1307.
    https://doi.org/10.1016/S0010-938X(00)00116-5

13. Liang, J., Srinivasan, P.B., Blawert, C., Stormer, M., et al., *Electrochim. Acta*, 2009, vol. 54, pp. 3842−3850.
    https://doi.org/10.1016/j.electacta.2009.02.004

14. Urban, M., The University of Manchester, 2014.

15. Kazanski, B., Kossenko, A., Zinigrad, M., and Lugovskoy, A., *Appl. Surf. Sci.*, 2013, vol. 287, pp. 461−466.
    https://doi.org/10.1016/J.APSUSC.2013.09.180

16. Kirkland, N.T., Birbilis, N., and Staiger, M.P., *Acta Biomater.*, 2012, vol. 8, pp. 925−936. .
    https://doi.org/10.1016/j.actbio.2011.11.014

17. Xin, Y., Hu, T., and Chu, P.K., *Corros. Sci.*, 2011, vol. 53, pp. 1522−1528.
    https://doi.org/10.1016/j.corsci.2011.01.015

18. Agarwal, S., Curtin, J., Duffy, B., and Jaiswal, S., *Mater. Sci. Eng., C*, 2016, vol. 68, pp. 948−963.
    https://doi.org/10.1016/j.msec.2016.06.020

19. Liang, J., Guo, B., Tian, J., Liu, H., et al., *Appl. Surf. Sci.*, 2005, vol. 252, pp. 345−351.
    https://doi.org/10.1016/j.apsusc.2005.01.007

20. Atrens, A., Song, G.-L., Shi, Z., Soltan, A., et al., *Reference Module in Chemistry, Molecular Sciences and Chemical Engineering*, Reedijk, J., Kakeya, H., Lammertsma, K., Marquardt, R., Eds., Amsterdam: Elsevier, 2017, pp. 1−20.
    https://doi.org/10.1016/B978-0-12-409547-2.13426-2

21. Zhang, X., Zhang, K., Deng, X., Li, H., et al., *Prog. Nat. Sci.*, 2012, vol. 22, pp. 169−174.
    https://doi.org/10.1016/j.pnsc.2012.03.014